Supporting Information for

Ultrafast Interfacial Energy Transfer and Interlayer Excitons in Monolayer WS_2 and $CsPbBr_3$ Quantum Dots Heterostructure

Han Li, [a] Xin Zheng,[b,c] Yu Liu, [a] Zhepeng Zhang, [d] Tian Jiang *,[a,b]

[a]College of Opto-Electronic Science and Engineering, National University of Defense Technology, Changsha 410073, P. R. China.

[b]Interdisciplinary Center of Quantum Information, National University of Defense Technology, Changsha 410073, P. R. China.

[c]State Key Laboratory of High Performance Computing, National University of Defense Technology, Changsha 410073, P. R. China.

[d]Center for Nanochemistry (CNC), Beijing Science and Engineering Center for Nanocarbons, Beijing National Laboratory for Molecular Sciences, College of Chemistry and Molecular Engineering, Academy for Advanced Interdisciplinary Studies, Peking University, Beijing 100871, P. R. China.

*tjiang@nudt.edu.cn

Fig. S1a is the scanning electron microscope (SEM) image and the thickness of WS_2 is 0.76 nm measured by atomic force microscope (AFM). Raman spectra in Fig. S1b illustrates a 62.6 cm^{-1} separation between in-plane E^1_{2g} mode and out-of-plane A_{1g} mode. Both AFM and Raman measurement results indicate ML WS_2 samples. And the average size of $CsPbBr_3$ QDs is 11 nm, also by SEM image shown in Fig. S1c and statistics in Fig. S1d. AFM measurements of $CsPbBr_3$ QDs on bare sapphire substrate and prapared WS_2 sample are shown in Fig. S1e and Fig. S1f, where The $CsPbBr_3$ QDs densities are approaching.

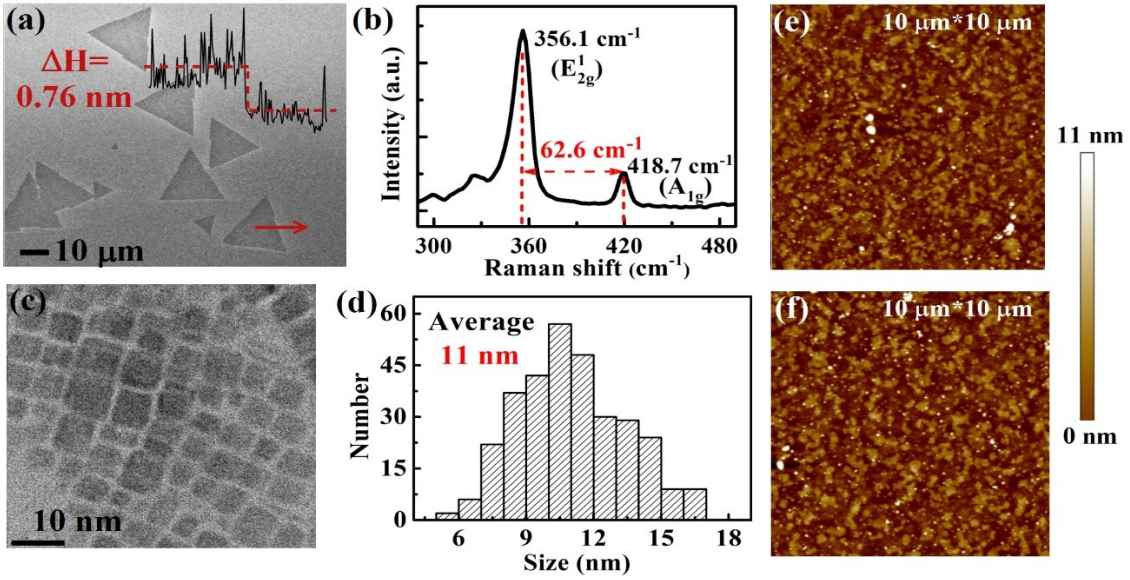

Fig. S1 (a) SEM image of ML WS_2, scale bar: 10 μm, red marked arrow: AFM measurement path. The stair-like fall of 0.76 nm height indicates ML WS_2. (b) Raman spectra of the WS_2 sample under 532 nm continuous wave excitation. (c) SEM image of $CsPbBr_3$ QDs with scale bar of 10 nm. (d) Statistics of $CsPbBr_3$ QDs size. Average size: 11 nm. (e)-(f) AFM measurements of $CsPbBr_3$ QDs on (e) bare sapphire substrate and (f) prapared WS_2 sample. The white dots on the surface are $CsPbBr_3$ QDs with average 11 nm size. $CsPbBr_3$ QDs densities in (e) and (f) are approaching. AFM scanning areas: 10 μm*10 μm.

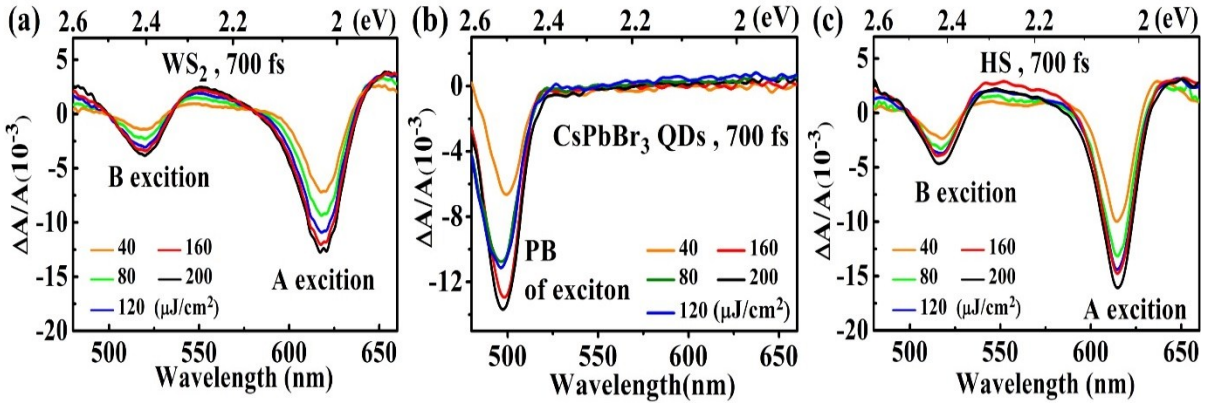

Fig. S2 (a)-(c) TAS signals of pristine ML WS_2, $CsPbBr_3$ QDs and the HS at 700 fs pump-probe time delay, with the pump fluence from 40 to 200 μJ/cm^2.

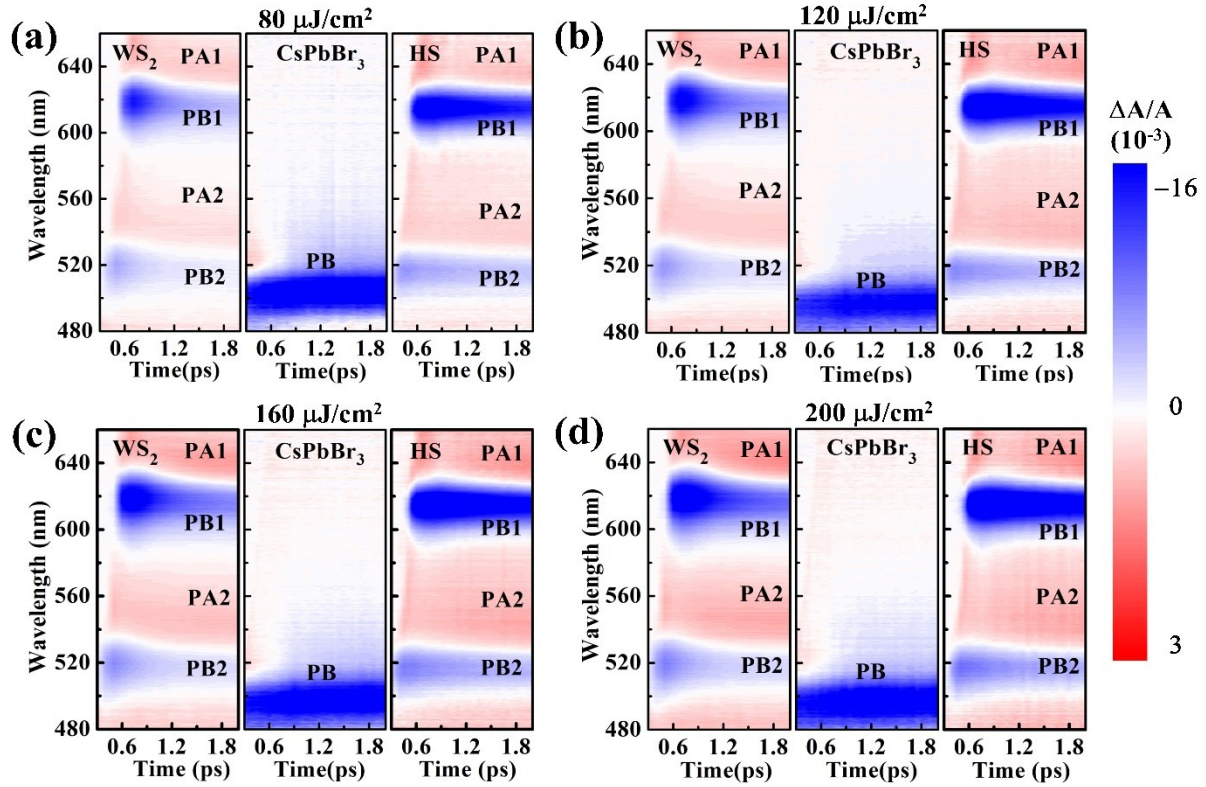

Fig. S3 2D pseudo-color maps of TAS measurements within first 5 ps time delay for pristine WS_2 in upper row, and the HS in lower row, with 80, 120, 160 and 200 μJ/cm^2 pump fluence. In HS, no obvious PB signals of excitons in $CsPbBr_3$ QDs appear, while PB1 in WS_2 layer are much enhanced.

The PB1 amplitude increases by an ultrafast energy transfer process from $CsPbBr_3$ QDs as analyzed in main text. The PB2 amplitude also increases somehow but not so much as PB1 region does when $CsPbBr_3$ QDs are applied. We attribute these different increments of to naturally unique band alignments between WS_2 and $CsPbBr_3$ QDs. From the view of band alignments in the HS, B exciton fluence may not increase. But we do observe a relative enhancement of PB2 signals and assign this to a transform of $CsPbBr_3$ excitons by probable ultrafast Auger scattering or Förster energy transfer from $CsPbBr_3$ excitons to B excitons in WS_2, which also weakens PB effect of $CsPbBr_3$ exciton somehow. But with a higher energy, some B excitons may transpose into A excitons via electroacoustic interactions as an "intra-material transition" process, which decreases the PB2 amplitude. On the other hand, there is an "inter-material transition" process of holes in B excitons. With 400 meV energy lower than VBM of $CsPbBr_3$, a fraction of holes on VBM2 of WS_2 "jump" across the interface, which is regarded as an interlayer transfer process that possibly induces interlayer excitons (IEs).

The enhancement levels of maximum PB1 and PB2 amplitude both tend to be fixed constants when pump fluence increases, as shown in Fig. S4f. There seems to be a threshold value of exciton fluence allowed in a material system somehow, whether individual material or combined HS. Transient exciton fluence over this threshold value, by drastic optical or electric excitations, may trigger some ultrafast nonradioactive channels which then decreases exciton fluence to "normal" threshold level rapidly. Given finite optical thickness of samples, this is also called as a saturated absorption mechanism in some steady-state situations,[1,2] which influences the whole efficiency a lot in semiconductor lasers and other light-emitting devices.[3,4]

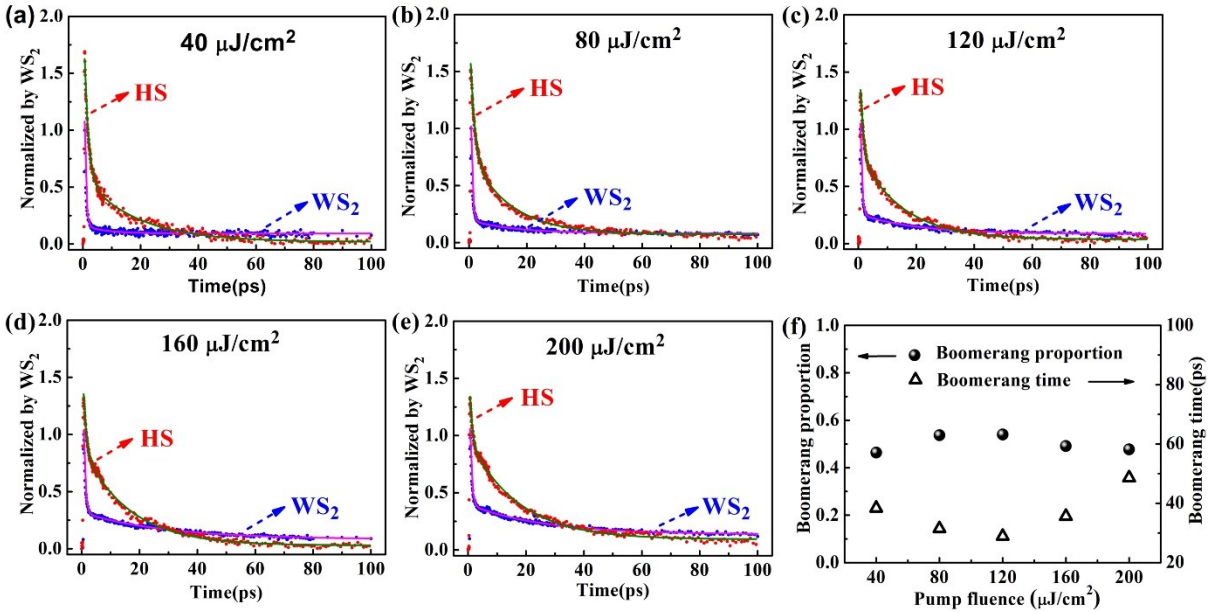

Fig. S4 Dynamical evolutions of PB1 signals of pristine WS_2 and the HS, with 40, 80, 120 and 200 μJ/cm^2 pump fluence. All data are normalized by corresponding PB1 signals of pristine WS_2. (a)-(e) Evolutions of PB1 signals in the HS. Rising times of PB1 signals are ~300fs in both pristine WS_2 and the HS. (f) Calculated boomerang time and ratio of interlayer excitons in the HS.

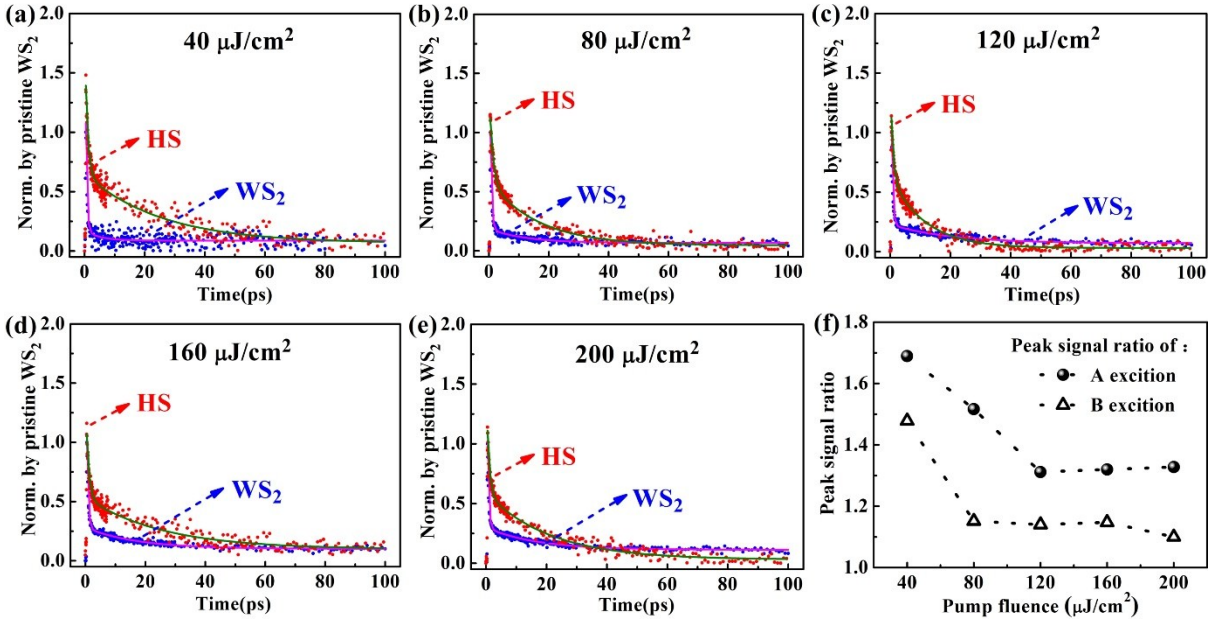

Fig. S5 Dynamical evolutions of PB2 signals of pristine WS_2 and the HS, with 40, 80, 120 and 200 μJ/cm^2 pump fluence. All data are normalized by corresponding PB2 signals of pristine WS_2. (a)-(e) Evolutions of B exciton resonance signal amplitudes in the HS. Rising times of PB2 signals are ~300fs in pristine WS_2 and the HS. (f) Calculated maximum amplitude ratios of PB1 and PB2 signals between pristine WS_2 and the HS, both showing to be saturated as pump fluence increases. And PB1 maximum increases by 69% at most in the HS under 40 μJ/cm^2 pump fluence. Noticing that fitted results for PB2 signals are less precise compared with PB1 signals.

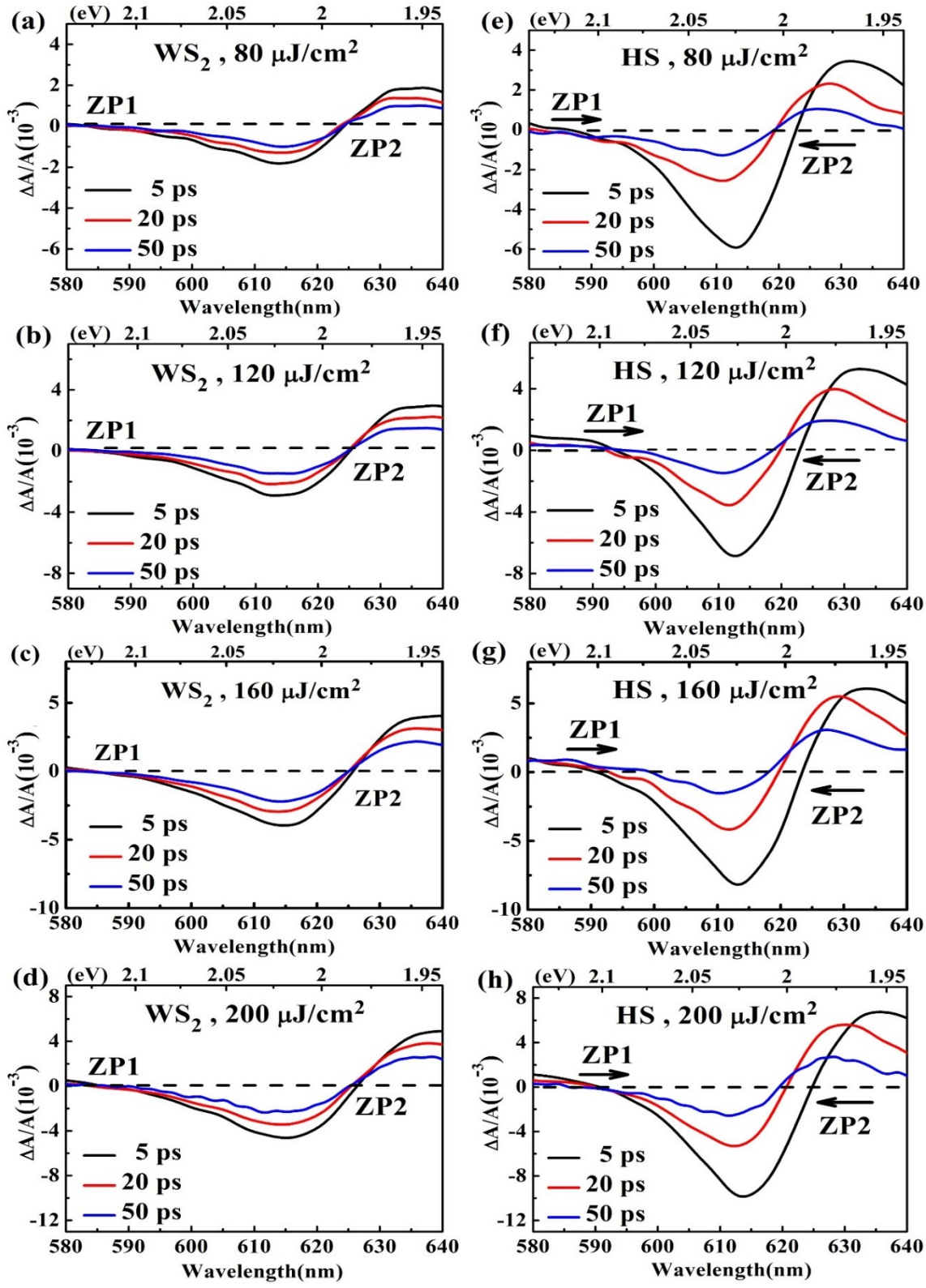

Fig. S6 TAS signals around A exciton resonance in pristine WS_2, and the HS, with 40, 80, 120 and 200 μJ/cm^2 pump fluence. (a)-(d) Under the same pump fluence, ZP1 and ZP2 nearly stay fixed at a same wavelength position with time in pristine WS_2. (e)-(f) ZP1 (ZP2) usually red-shifts (blue-shifts) with time in the HS. The wavelength width between ZP1 and ZP2 decreases with time in the HS, which is relatively smaller than that in pristine WS_2 under the same circumstance.

After 100ps time scale (≈ 3 lifetimes of interlayer excitons), there is not many interlayer excitons left, which means their influence on A exciton resonance decreases. So the difference between ZPs tend to be a constant after a long carrier reconbination time. TAS spectrum around A exciton resonance in pristine WS_2 and the HS under 200 uJ/cm^2 is shown in Fig. S7. After 100 ps in the HS, the ZPs positions in TAS stay nearly unchanged, which is an intrinsic feature of A exciton resonance.

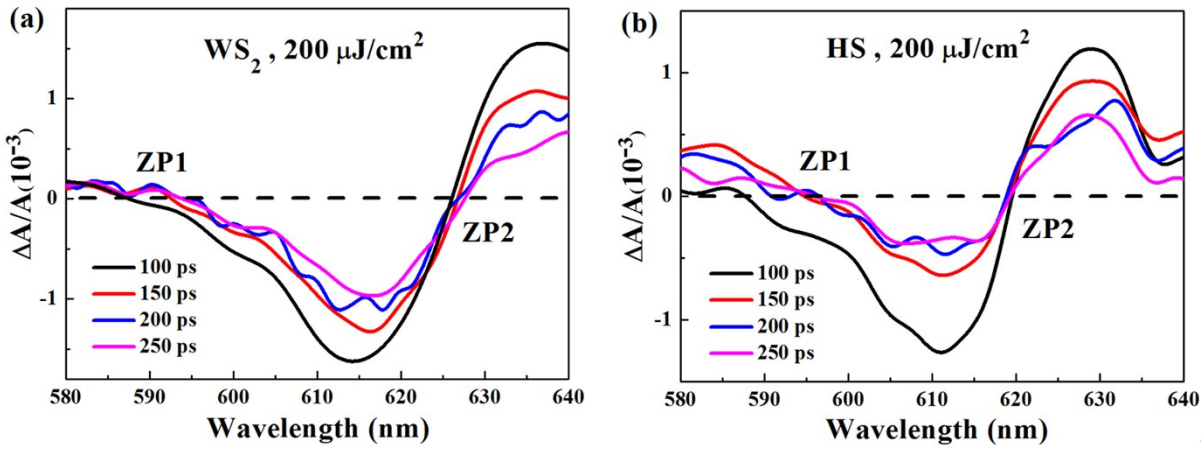

Fig. S7. TAS spectrum around A exciton resonance in (a) pristine WS_2 and (b) the HS under 200 uJ/cm^2. After 100 ps in the HS, the ZPs positions in TAS stay nearly unchanged, which shows A exciton resonance feature due to interlayer exciton fluence decrement.

Table S1 Dynamical time parameters of PB1 signals in pristine WS_2 and the HS, respectively. All recombination time parameters are well fitted as biexponential.

pump fluence (μJ/cm^2)	pristine WS_2				the HS			
	A_1 (*10^{-3})	A_2 (*10^{-3})	$T_{WS2,fast}$ (ps)	$T_{WS2,slow}$ (ps)	A_1 (*10^{-3})	A_2 (*10^{-3})	$T_{HS,fast}$ (ps)	$T_{HS,slow}$ (ps)
40	3.95 (65%)	2.12 (35%)	0.48	33.2	9.59 (93.4%)	0.67 (6.6%)	1.29	17.8
80	4.57 (50.1%)	4.56 (49.9%)	0.49	36.5	11.01 (81.4%)	2.51 (18.6%)	1.39	16.9
120	4.80 (44.3%)	6.04 (55.7%)	0.52	33.9	11.46 (80.6%)	2.76 (19.4%)	1.02	15.6
160	4.46 (38.1%)	7.25 (61.9%)	0.53	34.4	11.38 (73.6%)	4.08 (26.4%)	0.94	17.5
200	4.15 (33.5%)	8.23 (66.5%)	0.6	44.4	10.36 (63%)	6.08 (37%)	0.96	23.2

Table S2 Dynamical time parameters of PB2 signals in pristine WS_2 and the HS. All recombination time parameters are fitted as biexponential. Noticing that fitted dynamical time parameters for PB2 signals are less precise and more various, since signals for PB2 signals are rather weaker compared with PB1 signals. When A_2 is zero in pristine WS_2 at 40 μJ/cm^2, its corresponding time $T_{WS2,Slow}$ cannot be obtained because the fitting model is changed from bi-exponential into mono-exponential.

pump fluence (μJ/cm^2)	pristine WS_2				the HS			
	A_1 (*10^{-3})	A_2 (*10^{-3})	$\mathbf{T_{WS2,fast}}$ (ps)	$\mathbf{T_{WS2,slow}}$ (ps)	A_1 (*10^{-3})	A_2 (*10^{-3})	$\mathbf{T_{HS,fast}}$ (ps)	$\mathbf{T_{HS,slow}}$ (ps)
40	2.07 (100%)	0 (0%)	0.4	----	1.69 (55.3%)	1.37 (44.7%)	0.85	26.9
80	2.78 (81.1%)	0.65 (18.9%)	0.37	23.1	2.01 (51%)	1.93 (49%)	0.79	18.2
120	3.28 (80.6%)	0.79 (19.4%)	0.4	27.3	2.15 (46.3%)	2.49 (53.7%)	0.76	11.3
160	3.54 (79.2%)	0.93 (20.8%)	0.45	30.7	2.32 (45.2%)	2.81 (54.8%)	0.75	10.6
200	4.06 (78.1%)	1.14 (21.9%)	0.43	30	2.72 (48%)	2.95 (52%)	0.8	16.8

Discussions about many-body and bimolecular effect in WS_2 and the HS

Actually, TAS measurements under 40-200 μJ/cm^2 are actually out of linear regime, which can be seen from Fig. S8 below. And thus many-body effects must be taken into consideration in both WS_2 and the HS. By comparing Sun's model[3] with our actual experimental results, we've found that there are some differences that should be claimed. Firstly, ultrafast hot carrier cooling processes are observed and measured to be 400-600 fs in WS_2 and ~1 ps in the HS (in Table S1 and Table S2), which are absent in Sun's model. Secondly, the ratio of the strength about slow recombination in WS2 and the HS increases with pump fluence, which is consist with the description of exciton-exciton annihilation process by Sun. But our time parameters of slow recombination processes vary with pump fluence in both WS2 and the HS (in Table S1 and Table S2), while exciton-exciton annihilation time is unchanged (6 ps) in Sun's paper.[3] Thirdly, photon-induced carriers are all generated in monolayer MoS2 in Sun's model. However, carriers are generated in both CsPbBr3 quantum dots and WS2 when our HS is formed. The difference of carrier density between CsPbBr3 and WS2 depends on charge transfer process in the heterointerface, which complexes the many-body effect in the HS. On the basis of Sun's model, we think that many-body effect mechanism partly contributes to carrier slow recombination behaviors in WS2 and the HS.

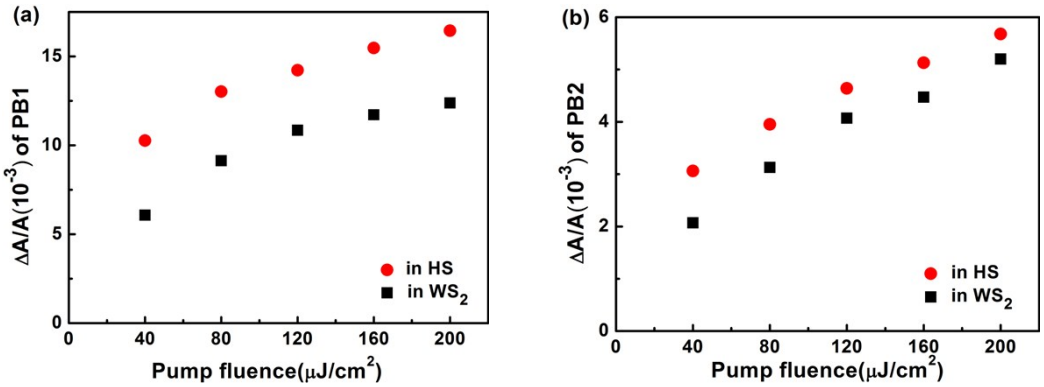

Fig.S8 The fluence-dependent absorption change of (a) PB1 and (b) PB2 in pristine WS_2 and the HS. PB1 and PB2 signals show a similar saturated increment behavior.

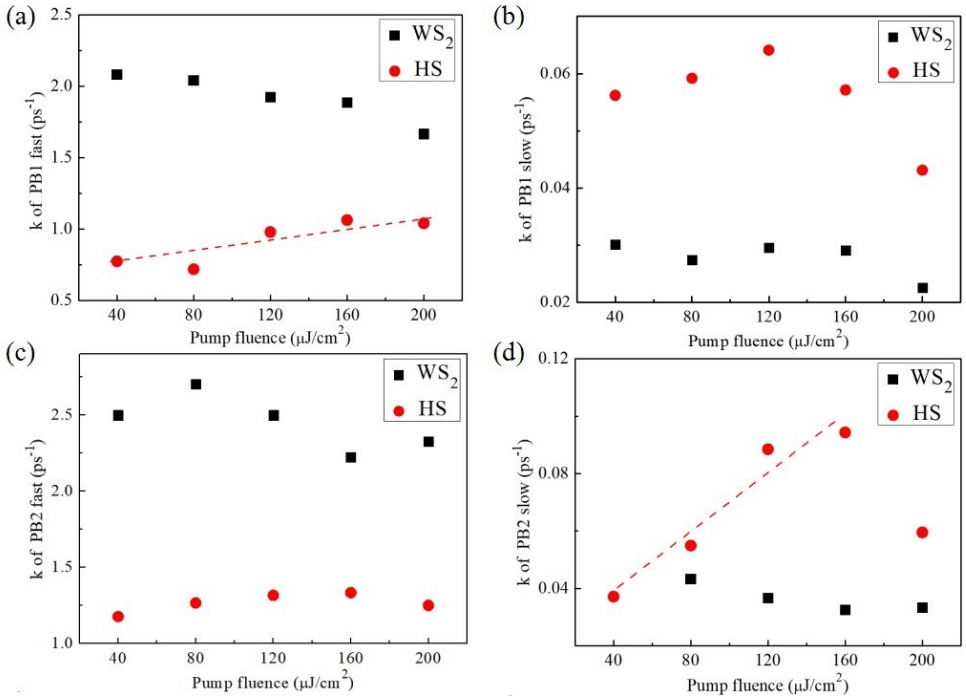

Fig. S9. Relaxation rate under different pump fluences in pristine WS_2 and the HS. (a) PB1 fast (b) PB1 slow (c) PB2 fast (d) PB2 slow

References

1. X. Zheng, Y. Zhang, R. Chen, X. Cheng, Z. Xu and T. Jiang, *Opt. Express*, 2015, **23**, 15616.
2. X. Zheng, R. Chen, G. Shi, J. Zhang, Z. Xu, X. Cheng and T. Jiang, *Opt. Lett.*, 2015, **40**, 3480.
3. D. Sun, Y. Rao, G. A. Reider, G. Chen, Y. You, L. Brézin, A. R. Harutyunyan and T. F. Heinz, *Nano Lett.*, 2014, **14**, 5625–5629.
4. K. Wei, X. Zheng, X. Cheng, C. Shen and T. Jiang, *Adv. Opt. Mater.*, 2016, **4**, 1993–1997.
5. V. V. Mayoral, T. Borzda, D. Vella, M. Prijatelj, E. A A Pogna, C. Backes, J. N Coleman, G. Cerullo, D. Mihailovic, *2D Mater.*, 2018, **5,** 015011.